JMEPEG (2017) 26:4056–4063
DOI: 10.1007/s11665-017-2840-2

1059-9495/$19.00

Microstructure, Hardness, and Corrosion Behavior of TiC-Duplex Stainless Steel Composites Fabricated by Spark Plasma Sintering

Ying Han, Wei Zhang, Shicheng Sun, Hua Chen, and Xu Ran

(Submitted September 29, 2016; in revised form May 14, 2017; published online July 25, 2017)

Duplex stainless steel composites with various weight fractions of TiC particles are prepared by spark plasma sintering. Ferritic 434L and austenitic 316L stainless steel powders are premixed in a 50:50 weight ratio and added with 3-9 wt.% TiC. The compacts are sintered in the solid state under vacuum conditions at 1223 K for 5 min. The effects of TiC content on the microstructure, hardness, and corrosion resistance of duplex stainless steel composites fabricated by powder metallurgy are evaluated. The results indicate that the TiC particulates as reinforcements can be distributed homogeneously in the steel matrix. Densification of sintered composites decreases with increasing TiC content. $M_{23}C_6$ carbide precipitates along grain boundary, and its neighboring Cr-Mo-depleted region is formed in the sintered microstructure, which can be eliminated subsequently with appropriate heat treatment. With the addition of TiC, the hardness of duplex stainless steel fabricated by powder metallurgy can be markedly enhanced despite increased porosity in the composites. However, TiC particles increase the corrosion rate and degrade the passivation capability, particularly for the composite with TiC content higher than 6 wt.%. Weakened metallurgical bonding in the composite with high TiC content provides the preferred sites for pitting nucleation and/or dissolution.

Keywords 434L, 316L, corrosion, spark plasma sintering, stainless steel, TiC

1. Introduction

Duplex stainless steel has been widely used in heat exchangers, petroleum refining, paper manufacturing, and ocean industry because of its excellent combination of high strength and toughness, good weldability, and superior resistance to local corrosion (Ref 1-3). The desirable properties of duplex stainless steel depend on a two-phase microstructure composed of nearly equal amounts of austenite and ferrite (Ref 4). Thus, duplex stainless steel has become a special class among stainless steels. In conventional manufacturing, duplex stainless steel is processed using different procedures, such as casting, forging, extrusion, or rolling (Ref 5). However, the thermal expansion coefficients and the deformation behaviors of constituent phases vary, and a secondary-phase precipitates on the grain boundaries, rendering the manufacturing process of duplex stainless steel rather complex. Powder metallurgy (PM) provides an excellent alternative to the production of duplex stainless steel. This technique involves a simple process and requires little machining. The method is also cost-effective and environment-friendly, particularly for small components. The more important properties of the PM include broad-spectrum composition design, microstructure control, as well as physical and mechanical property optimization. In recent years, research on duplex stainless steel fabricated by PM has drawn extensive attention (Ref 6-10), and sintered parts made by this material have been introduced to automotive appliances industries (Ref 11, 12).

However, the potential application of PM stainless steel is often constrained by low hardness and poor wear resistance (Ref 9, 10). To address these disadvantages, significant effort has been directed toward enhancing the mechanical properties of PM stainless steels. Studies (Ref 13-19) indicate that the addition of hard ceramic particles (Al_2O_3, TiB_2, TiC, Y_2O_3, etc.) into stainless steels practically strengthens the PM composites, particularly enhancing hardness and abrasion resistance. Among these hard ceramic particles, TiC is regarded as a suitable reinforcement for steel matrix composites owing to its high hardness, low density, good wettability, and satisfactory stability with the matrix. Reinforcement by TiC particles have been shown to markedly improve the abrasion resistance of PM 316L and 465 stainless steels (Ref 16, 17). However, the addition of TiC generally leads to a decrease in the corrosion resistance of PM stainless steels (Ref 20). TiC particles, as the distinct constituent with the base metal, allow for corrosion on the interface. Moreover, TiC promotes the presence of pores in the PM composites, which can magnify the adverse effect on corrosion resistance. Therefore, high density and good metallurgical bonding between the base metal and TiC particles are necessary to produce TiC particle-reinforced PM stainless steels. Kazior et al. (Ref 21) employed boron-activated sintering to enhance densification by the formation of a persistent liquid phase. Lin and Xiong (Ref 16) prepared a high-density TiC-316L stainless steel composite by warm compaction and microware sintering. A maximum relative

Ying Han, Shicheng Sun, Hua Chen, and **Xu Ran**, Key Laboratory of Advanced Structural Materials, Ministry of Education, Changchun University of Technology, Changchun 130012, China; and **Wei Zhang**, State Key Laboratory for Mechanical Behavior of Materials, Xi'an Jiaotong University, Xi'an 710049, China. Contact e-mail: hanying_118@sina.com.

density of 94.8% was obtained in the composite with 5 wt.% TiC, which exhibited improved mechanical property relative to steel processed using conventional methods.

Spark plasma sintering (SPS), also referred to as pressure-assisted fast electric sintering, is an advanced sintering technique that combines high heating rates with high pressure to consolidate powder compacts to a high density within a short period (Ref 22-25). Compared with conventional sintering techniques, such as hot pressing and hot isostatic pressing, SPS exhibits a high degree of densification, grain refinement, low sintering temperature, and shorter sintering time. Therefore, SPS as preparation process of TiC-reinforced stainless steel composites exhibits potential for enhanced densification and mechanical properties. However, studies on this aspect have rarely been reported, and the related experimental data remain lacking.

Powders for sintering multiphase composites can be produced using three methods: (1) using pre-alloyed powders with a required composition, (2) mixing base metal powders with alloying elements or (3) combining various single-phase alloy powders in a specific ratio to obtain the required microstructure (Ref 26-28). The last method is applied in this study to obtain a duplex microstructure using ferritic 434L and austenitic 316L stainless steel powders because it can be easily achieved with different mixtures. The main objective is to reveal the effects of TiC addition on the densification, microstructure, hardness, and electrochemical corrosion behavior of TiC-reinforced duplex stainless steel fabricated by SPS.

2. Experimental Procedure

The commercial water-atomized stainless steel powders used in this study were 316L and 434L, and the chemical compositions of which are shown in Table 1. The 316L powder exhibited the following physical characteristics: apparent density, 3.9 g/cm^3; flow rate, 30 s/50 g; and average particle size, 38 μm. The 434L powder exhibited the following physical characteristics: apparent density, 3.7 g/cm^3; flow rate, 32 s/50 g; and average particle size, 35 μm.

To evaluate the influence of the TiC particle on the microstructure and property of the sintered duplex stainless steel, different proportions of TiC (0, 3, 6, 9 wt.%) powder (average 0.9 μm in size) were added into the mixed stainless steel powders, with the 434L to 316L powders ratio as set to 50:50 by weight. The composite powders were dry-milled in stainless steel vials for 12 h by using a planetary ball mill with a rotational speed of 300 rpm. GCr 15 steel was used as the ball material. The ball-to-powder weight ratio was optimized at 10:1. Figure 1 shows morphology of the milled composite powders. As shown, all steel powders exhibit an irregular shape with better compactness and sinterability. In Fig. 1(b), fine TiC particles adhere to large-particle ferritic and austenitic powder surfaces, which results in the steel powders being covered with an outer layer of TiC particles. The expected composite powders were obtained.

In the present study, the TiC-reinforced duplex stainless steels were prepared by SPS. The composite powders with various TiC contents were pre-compacted in a graphite mold under a pressure of 10 MPa. The pre-compacted pieces were sintered using an SPS device at 1223 K and pressure of 40 MPa for 5 min under vacuum condition. The initial heating rate was set to 100 K/min. To minimize the friction between the die walls and the powder, a graphite sheet was used, which also facilitated the ejection of specimens after sintering. The sintered specimens were allowed to cool to room temperature with the furnace, and dense disks 20 mm in diameter and 3 mm in height were obtained. After sintering, solution heat treatments were performed at 1423 K for 60, 90, and 120 min to homogenize the microstructure, followed by water quenching. Setting the solution treatment temperature at approximately 1423 K is to make sure that the precipitated carbides can be eliminated.

The sintered density of the TiC-reinforced duplex stainless steel fabricated by PM was measured using a density determination kit, which follows the Archimedes principle. The theoretical density of the composite was calculated based on the "rule of mixture" from the densities of raw powders. The relative density was calculated using the formula: sintered density/theoretical density $\times$ 100%. A Vickers hardness tester was used, with a load of 100 N for 15 s of indentation time; an average of 5 readings was reported.

Microstructural observation and chemical composition analysis were conducted by using scanning electron microscopy (SEM) with energy dispersive x-ray spectroscopy (EDS). Etching with ferric chloride and electrochemical etching with oxalic acid were employed (Ref 27). Phase identification of composites was performed by x-ray diffraction (XRD) with Cu Ka radiation with a step size of 0.02/s.

Electrochemical tests were performed in a 3.5 wt.% NaCl solution at room temperature. Polarization curves were measured in a 3 electrode cell composed of a specimen as a working electrode, a Pt wire as a counter electrode, and a saturated calomel reference electrode. The specimens were cut, measuring 10 mm $\times$ 10 mm $\times$ 2.5 mm, coated with epoxy resin, leaving a 1 cm^2 surface exposed to the testing solution. The exposed surfaces were degreased in benzene, cleaned ultrasonically, and subsequently washed with distilled water. Before the polarization curves were measured, the specimens were immersed in a testing solution for 15 min until a stable value of the open circuit potential was reached. The potential was scanned from -1.5 to $+2.0$ V at a sweep rate of 0.2 mV/s. All electrochemical tests were repeated 3 times to ensure reproducibility. The parameters presented are the average values. To characterize the preferential pit location, the specimens were cleaned and analyzed after

Table 1 Chemical compositions of 316L and 434L stainless steel powders (wt.%)

Type	C	Cr	Ni	Mo	Si	Mn	O	Fe
316L	0.023	16.90	12.90	2.05	0.90	0.17	$<$0.10	Bal.
434L	0.020	17.29	…	1.92	0.67	0.20	$<$0.10	Bal.

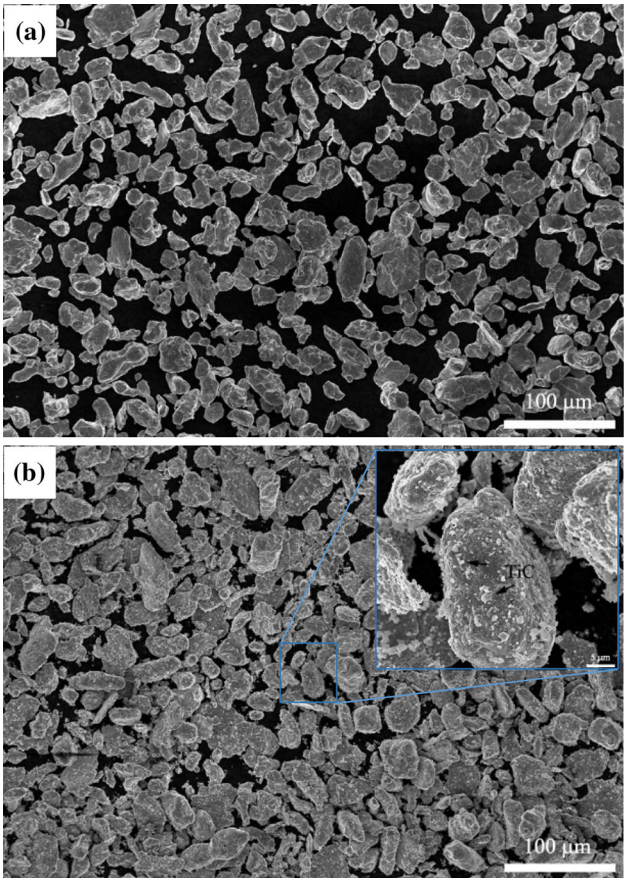

Fig. 1 SEM micrographs of milled composite powders with different TiC contents: (a) 0 wt.% TiC; (b) 9 wt.% TiC

being immersed in the solution of 6 wt.% $FeCl_3$ and 0.05 mol/L HCl for 6 h.

3. Results and Discussion

Figure 2 shows the variations in sintered density and relative density with the TiC content of TiC-duplex stainless steel composites fabricated using 316L and 434L steel powders. The errors fall within the ±0.2%-±1.5% range. By using the same sintering process, the sintered density of composites decreases owing to the addition of light TiC. The relative density of composites also decreases with increasing TiC content. The composite with on TiC added exhibits a relative density of 98.7%, which is much higher than that obtained using conventional hot-pressed sintering (Ref 7). A slightly decreased relative density of 96.9% is observed for the sintered composite with 3 wt.% TiC. The density decreases rapidly when TiC content is more than 6 wt.%. For example, the relative density of sintered composite with 9 wt.% TiC is only 92.7%. The decrease in the relative density of the composites suggests that densification can be effectively lowered by increasing the TiC content added in the initial mixtures.

The XRD patterns of sintered composites with different TiC contents are shown in Fig. 3. The major diffraction peaks of austenite (γ) and ferrite (α) phases are presented in all composites. As TiC is added, its diffraction peaks are detected, and the diffraction intensity increases gradually as intended.

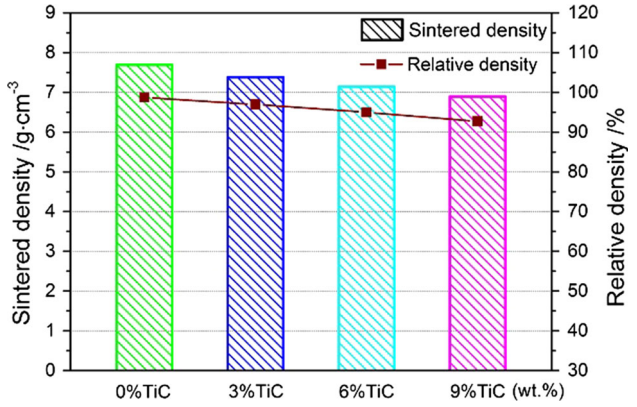

Fig. 2 Sintered density and relative density of studied composites with different TiC contents

However, apart from the predictable peaks, the slight peaks of undesirable phases are observed for all the composites and are identified as $M_{23}C_6$ carbides, which enrich alloying elements of Cr and Mo. SEM micrographs of sintered composites with different TiC contents are shown in Fig. 4. For the TiC-free sintered composite (Fig. 4a), the microstructure exhibits homogeneous sintered grains and good metallurgical bond at the interface between the ferrite and austenite phases; however, a small number of spherical pores are present. Meanwhile, a large number of extra phases exhibiting reticular shapes are precipitated from the ferritic grain boundaries, which are marked in the figure. Figure 3 shows that this phase represents $M_{23}C_6$ carbide. By careful observation, in the austenitic zone, carbides (reticular dark-gray region, marked in Fig. 4a) can also be found. The amount of all precipitated phases in this sample reaches 13.5%. Meanwhile, as shown in Fig. 4(b) and (c), the TiC particulates are distributed homogeneously in the composites when the TiC weight content changes from 3% to 9%. This occurrence is related to good dispersion of TiC particulates in the mixed powders during milling. The sample with 3 wt.% TiC has a wholly metallurgical bond zone between the steel matrix and TiC with no apparent interface. However, as TiC content increases, the bonding boundaries accommodate a considerable amount of micro-voids. The morphological observation is consistent with the values of relative density (Fig. 2). The reason is that the probability of TiC-TiC interaction and agglomeration of TiC at the interfaces is increased with increasing TiC content (Ref 16, 17). This occurrence results in the formation of micro-voids and reduction in interface bonding between the TiC particles and the duplex matrix, thereby decreasing the relative density of composites. Surprisingly, for the composite with 3 wt.% TiC (Fig. 4b), only a small amount of $M_{23}C_6$ carbides is formed on the ferritic grain boundaries, and little precipitation in the austenitic zones can be observed. A further increase in TiC content to 6 wt.% favors the nucleation and growth of $M_{23}C_6$ carbide in ferritic phases, as shown in Fig. 4c, and the reticular structure is gradually developed along the grain boundaries. When the TiC addition reaches 9 wt.% (Fig. 4d), the sintered microstructure presents a considerable amount of precipitates, which are found in both austenite and ferrite. In addition, the obvious growth of grains in the matrix can be observed with the increase in TiC content.

To identify the differences in the chemical compositions of phases during the precipitation of carbides, EDS was conducted. The results are presented in Table 2; corresponding

points also appear in Fig. 4(b) and (d). As shown, the carbides (marked as B, D, and F) precipitated from either ferrite or austenite are rich in Cr and Mo without Ni. Cr-Mo-depleted regions near carbides, which exhibits considerably lower concentrations of Cr and Mo emerge, marked as C, E, and G

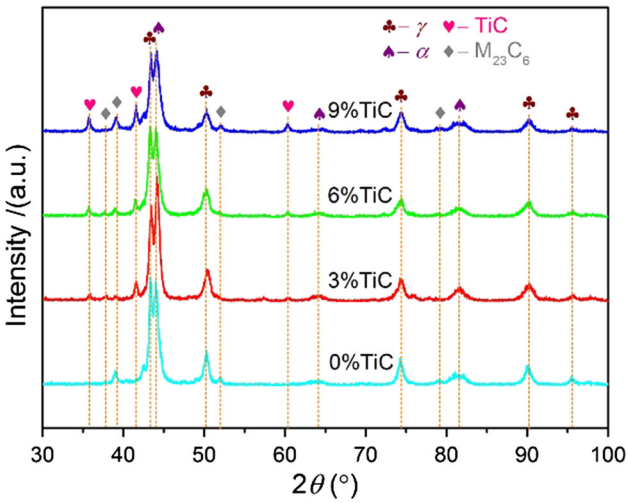

Fig. 3 XRD patterns of sintered composites with different TiC contents

areas because of the elements partitioned between carbides and matrix phases. Such microstructures generally lead to a drastic decrease in corrosion and mechanical properties of stainless steel. Post-sintered heat treatment is thus necessary to dissolve the undesirable phases into a solid solution and obtain a precipitate-free structure (Ref 6). The high current in SPS activates the surfaces of milled powders, which can promote not only the exchange of alloying elements but metallurgical bonding among the powders as well. Thus, the sintering temperature applied in SPS is often 200-300 K lower than that for traditional sintering. For the TiC-free sintered sample, obtaining a high relative density indicates the SPS technology can produce the compact duplex stainless steel, which reflects a good interaction between the interfaces of steel-based powders. With TiC addition, the formation of micro-voids caused by weakened TiC-TiC interaction and TiC agglomeration reduces the densification of the TiC-reinforced duplex stainless steel fabricated by PM. However, the sintering temperature of 1223 K used in this study is only located in the sensitive temperature range of ferritic or austenitic stainless steels, 1123-1353 K, and thus increases the possibility of precipitation of $M_{23}C_6$ carbide, namely byproduct. For SPS, the interface temperature of particles is considerably higher than the pre-set sintering temperature because of the microdischarge among different particles (Ref 29). SPS without cooling control and uniform thermal transmission inevitably results in secondary-phase precipita-

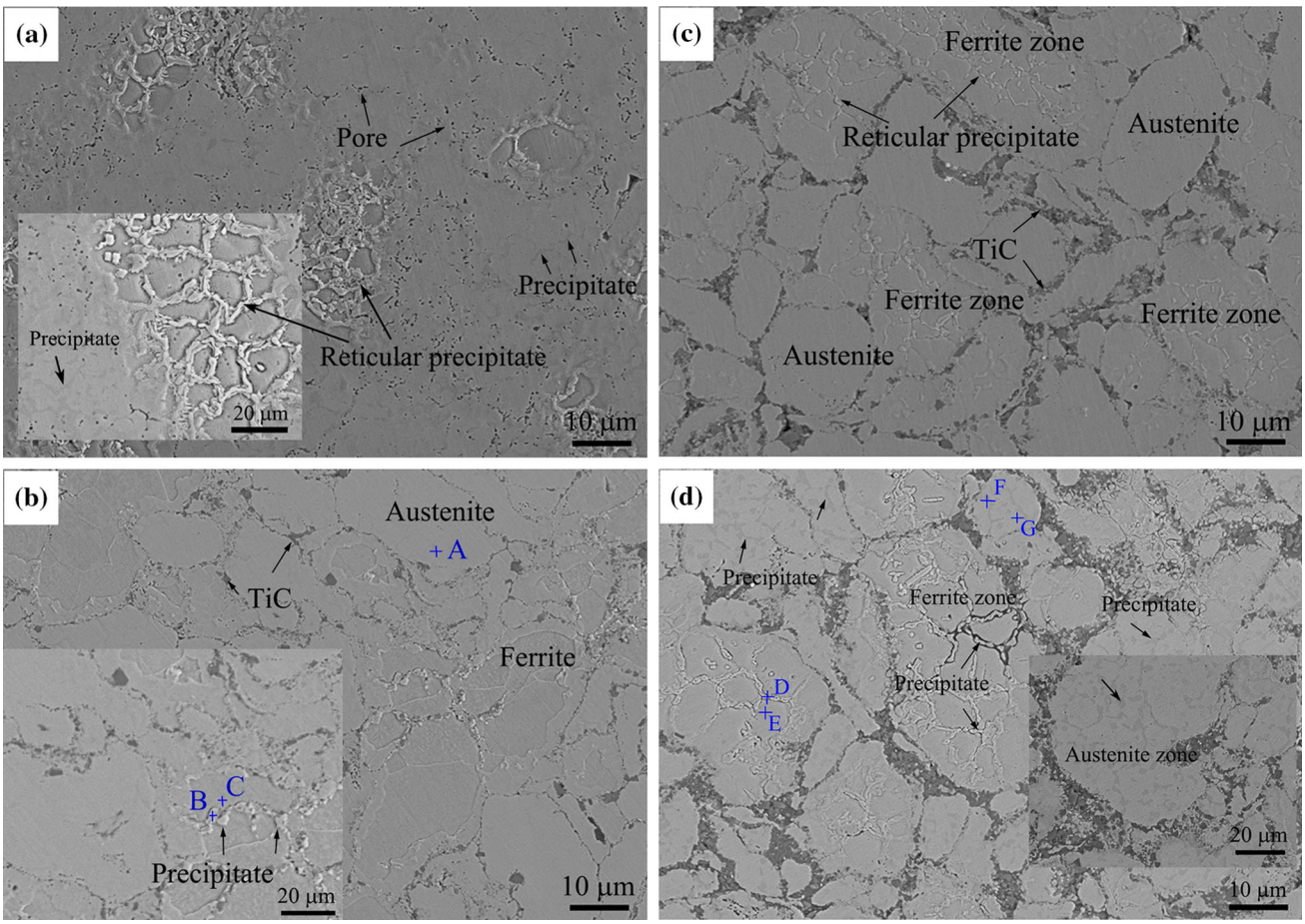

Fig. 4 SEM micrographs of sintered TiC-reinforced duplex stainless steel composites with (a) 0 wt.%; (b) 3 wt.%; (c) 6 wt.%; and (d) 9 wt.% TiC

tion in both ferrite and austenite. With increasing TiC content, the reaction on the bonding zones consumes a vast amount of energy supplied by SPS, thus lowering the driving force for the diffusion rates of alloying elements. Owing to greater atomic mobility in the open body-centered cubic ferrite structure, the carbide precipitation is first detected in the ferritic phases (Ref 7) (Fig. 4b and c). Once the phase boundaries are wholly encased by the TiC particles, they can strongly prevent heat transfer in the steel matrix during slow cooling. It provides sufficient time for the diffusion of alloying elements, which can facilitate the precipitation of undesirable precipitates. This occurrence explains the increased quantity of $M_{23}C_6$ carbides in the composites with 9 wt.% TiC.

The formation of $M_{23}C_6$ carbides and their neighboring alloying element depleted regions can deteriorate the corrosion resistance and mechanical properties of sintered stainless steels. Consequently, the solution treatment for this material is significant prior to application. The typical microstructures of the solutionized TiC-reinforced duplex stainless steels fabricated by PM with different holding time are shown in Fig. 5. As observed, the amount of $M_{23}C_6$ carbide is markedly decreased with increasing solution time, and the reticular structure of the precipitate evolves into the spot shape retained on the grain boundaries. The dependence of the $M_{23}C_6$ carbide volume fraction in the composites with different TiC contents on the solution treatment time is shown in Fig. 6. If sufficient holding time for the composites is applied (e.g., 120 min in this

Table 2 Chemical compositions of phases in composites corresponding to Fig. 4(b) and (d), as determined by EDS

		Elements concentration, wt.%				
Sample	**Selected area**	**Cr**	**Mo**	**Ni**	**Si**	**Fe**
3 wt.% TiC	A (in austenite)	16.57	2.23	12.78	0.85	67.57
	B (in ferrite)	47.51	5.42	…	…	47.07
	C (in ferrite)	12.11	1.42	…	0.5	85.97
9 wt.% TiC	D (in ferrite)	36.91	4.93	…	…	58.16
	E (in ferrite)	12.81	1.56	…	0.72	84.91
	F (in austenite)	46.65	5.8			47.55
	G (in austenite)	7.02	1.19	12.75	1.07	77.97

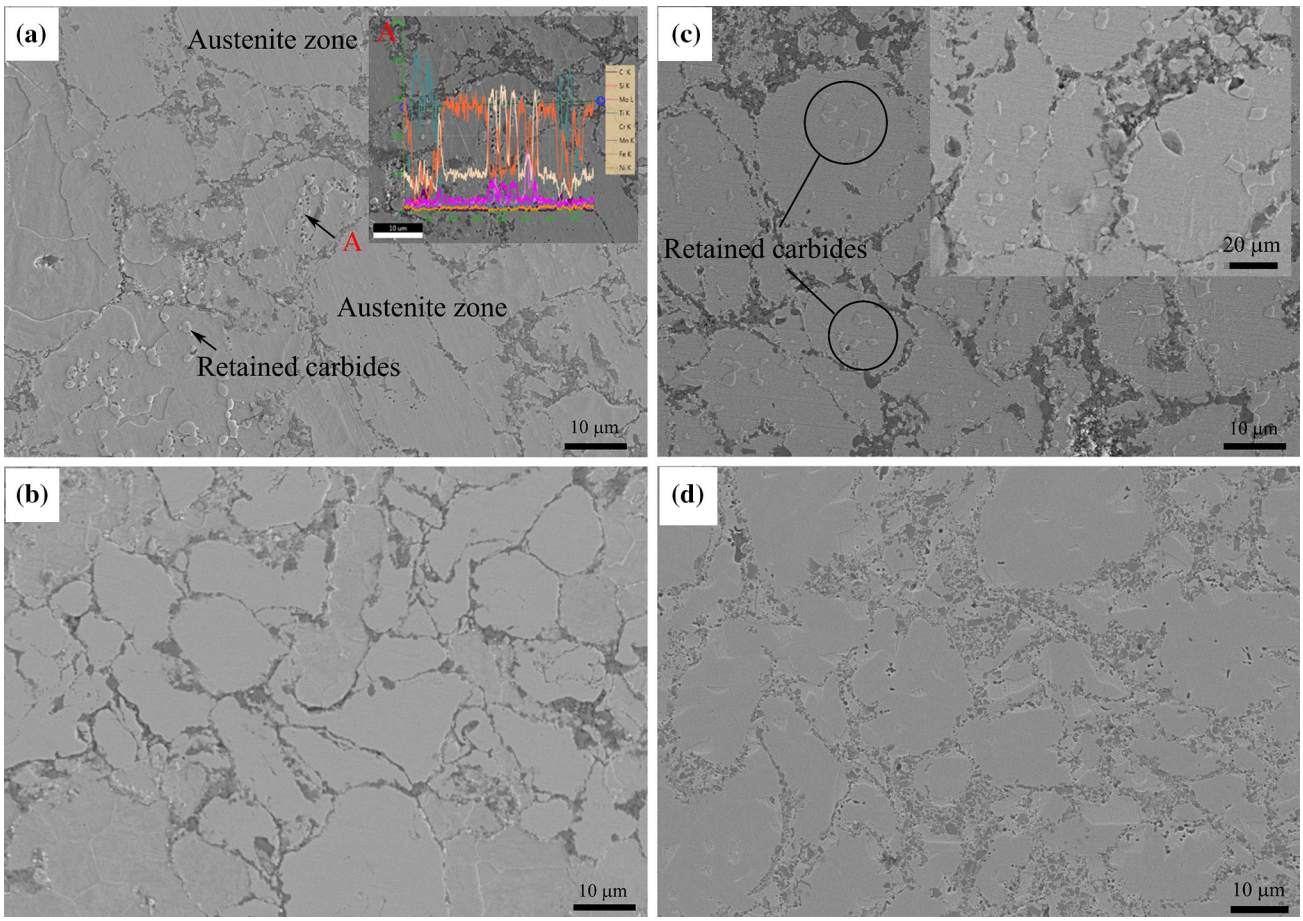

Fig. 5 Typical microstructures of heat-treated composites with different TiC contents: (a) 6 wt.% TiC for 60 min; (b) 6 wt.% TiC for 120 min; (c) 9 wt.% TiC for 60 min; and (d) 9 wt.% TiC for 120 min

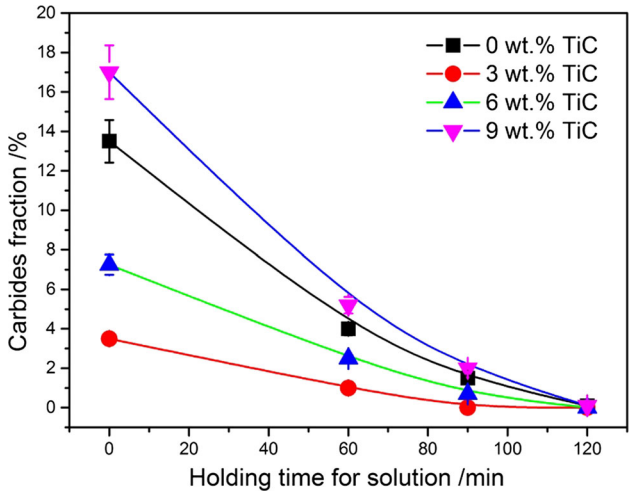

Fig. 6 Variation in volume fraction of precipitates for different amounts of TiC added

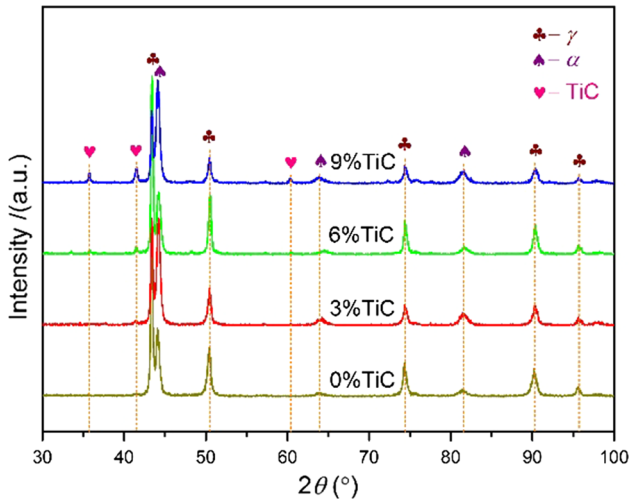

Fig. 7 XRD patterns of TiC-reinforced duplex stainless steel composites subjected to solution treatment for 120 min

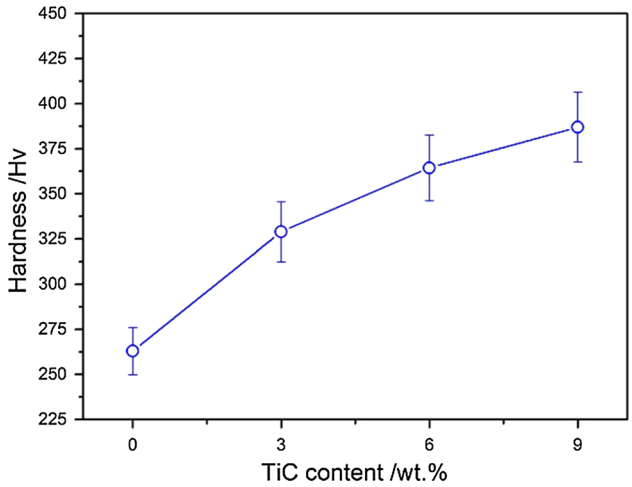

Fig. 8 Hardness of TiC-reinforced duplex stainless steel composites subjected to solution treatment for 120 min

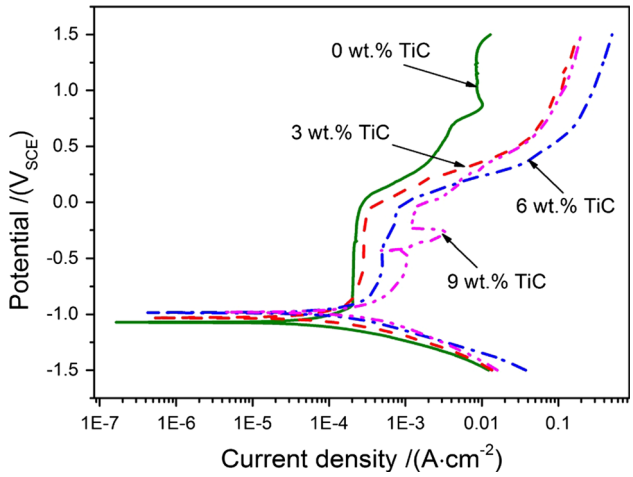

Fig. 9 Potentiodynamic polarization curves of TiC-reinforced duplex stainless steel fabricated by PM

Table 3 Electrochemical parameters obtained from polarization curves

Sample	E_{corr}, V	I_{corr}, μA/cm^2	I_{pass}, μA/cm^2	Porosity, %
0 wt.% TiC	−1.07	13.36	21.49	1.1
3 wt.% TiC	−1.04	18.36	28.61	2.7
6 wt.% TiC	−0.98	20.24	51.06	4.8
9 wt.% TiC	−0.98	32.29	1049.94	7.0

study), the undesirable phases can be dissolved. Figure 7 exhibits the XRD patterns of the composites after solution treatment at 1223 K for 120 min. The obtained microstructure consists of austenitic, ferritic, and TiC phases. No diffraction peaks of secondary phases, such as carbide, are found. In addition, the solution treatment benefits the metallurgical bonding of phase interfaces, and the open pores of heat-treated samples can be decreased. Figure 8 presents the variation in Vickers hardness with different amounts of TiC for the composites heat-treated for 120 min. This variation indicates that the hardness of composites increases with increasing TiC content. This behavior is attributed to the addition of TiC particles and their distribution around the phase boundaries caused by the increased hardness of TiC. To illustrate, hardness increases from 242 to 288 as the TiC weight fraction increases up to 3%. However, with the increase in TiC content to 9 wt.%, the hardness values of the composites exhibit a slower increase, which results from the reduction in the relative density of the composites. Generally, composites with increased TiC content also exhibit poor wear resistance because of reduced densification and weakened interface bonding (Ref 16).

Figure 9 shows the polarization curves of the solution-treated composites in a 3.5 wt.% NaCl solution. Table 3 presents the passive current density (I_{pass}), corrosion current density (I_{corr}), corrosion potential (E_{corr}), and porosity of heat-treated composites where a low potential indicates a high corrosion tendency, and increased current density implies increased corrosion rate. As shown in this figure, the composites with different TiC contents show a similar corrosion behavior in NaCl solution, and apparent passive characteristics are found on the polarization curves. I_{pass} values vary from

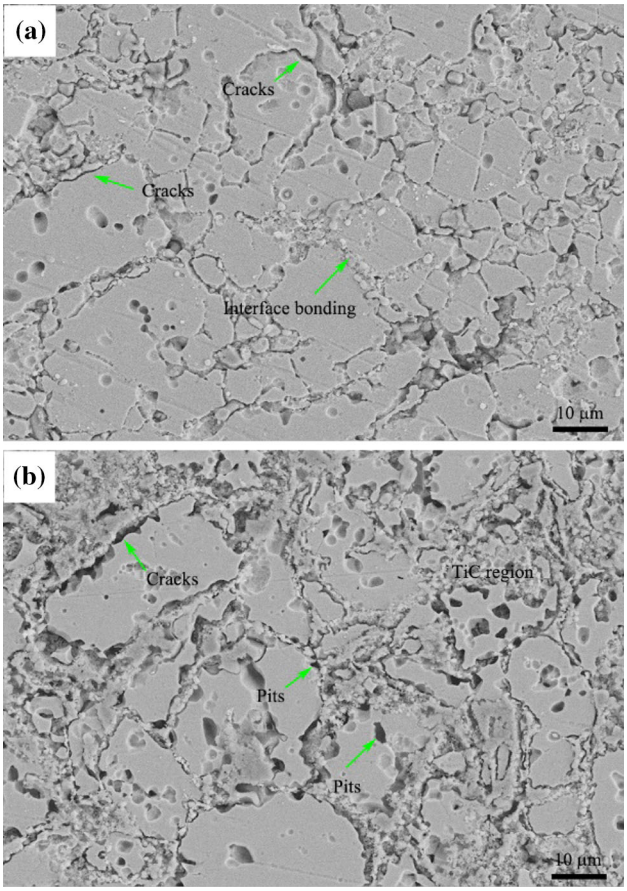

Fig. 10 Surface appearance of immersed samples with different TiC contents: (a) 3 wt.%; (b) 9 wt.%

21.49 μA to 1.05 mA with the addition of TiC. However, in the passive region, the current fluctuates between −0.63 and −0.24 V with increasing TiC content, which indicates the occurrence of repassivation and self-repair after the damage of passive film in the particular potential region. After passive range, rapid increase in current density occurs, and the passive layer is destroyed to accelerate pitting corrosion. Moreover, the differences in corrosion current density are clearly evident. I_{corr} values markedly increase with increasing TiC content although a change occurs in E_{corr} values, which shows that the large addition of TiC increases the susceptibility to corrosion. This increase indicates TiC addition reduces the corrosion resistance of duplex stainless steel fabricated by PM. The high current density in the PM stainless steels is related to the presence of pores caused by TiC addition, and generally, corrosive pits are initially formed in open porosity and then proceed to the interior of the pore (Ref 30). Figure 10 shows the surface appearance of immersed samples with different TiC contents. Pits and cracks along the phase boundaries are found to exhibit a markedly high density, which reveals that the phase boundaries between TiC and the matrix are preferential sites for corrosion attack after the duration of immersion.

4. Conclusions

In this study, the duplex stainless steels fabricated by PM with TiC addition were prepared by SPS. The applied sintering method and post-heat treatment allowed for manufacturing the TiC-duplex stainless steel composites with a uniform microstructure and satisfactory integrated properties. TiC addition can reduce the densification of the sintered composites, and relative density decreases rapidly when the TiC content exceeds 6 wt.%. During SPS, the $M_{23}C_6$ carbides are first precipitated along the grain boundaries of ferrite and then expand to the austenite with increasing TiC content, which causes the depletion of useful alloying elements Cr and Mo from the steel matrix. Appropriate heat treatment can be used to dissolve the precipitates and improve the densification of TiC-duplex stainless steel composites. The hardness of duplex stainless steel fabricated by PM can be markedly enhanced with TiC particles as composite reinforcements. However, the higher the amount of TiC, the lower is the corrosion resistance that can be obtained. More open pores caused by large amounts of TiC addition provide the preferred sites for pitting and/or dissolution. To summarize, the addition of 3 wt.% TiC in the matrix is considerably more effective, taking into consideration the microstructure, hardness, and corrosion resistance.

Acknowledgments

This work is supported by the National Natural Science Foundation of China (Nos. 51371038 and 51604034), the Scientific and Technological Planning Project of Jilin Province (Nos. 20150520030JH) and the Scientific and Technological Research Fund of Jilin Provincial Education Department during the Twelfth Five-year Plan Period (No. 2015-95).

References

1. D.N. Zou, Y. Han, W. Zhang, and G.W. Fan, Phase Transformation and Its Effects on Mechanical Properties and Pitting Corrosion Resistance of 2205 Duplex Stainless Steel, *J. Iron Steel Res. Int.*, 2010, **17**(11), p 67-72
2. P. Cizek, The Microstructure Evolution and Softening Processes During High-Temperature Deformation of a 21Cr-10Ni-3Mo Duplex Stainless Steel, *Acta Mater.*, 2016, **106**, p 129-143
3. Y.H. Yang, J.C. Cao, and Y. Gu, Investigation on the Solution Treated Behavior of Economical 19Cr Duplex Stainless Steels by Mn Addition, *Mater. Des.*, 2015, **83**, p 820-828
4. D.N. Zou, Y. Han, W. Zhang, and J.H. Yu, Sigma Phase Precipitation and Properties of Super-Duplex Stainless Steel UNS S32750 Aged At the Nose Temperature, *J. Wuhan Univ. Technol. Mater. Sci. Ed.*, 2011, **26**(2), p 183-186
5. Y. Han, D.N. Zou, Z.Y. Chen, G.W. Fan, and W. Zhang, InvESTIGATION on Hot Deformation Behavior of 00Cr23Ni4N Duplex Stainless Steel Under Medium-High Strain Rates, *Mater. Charact.*, 2011, **62**, p 198-203
6. L.A. Dobrzánski, Z. Brytan, M.A. Grande, M. Rosso, and E.J. Pallavicini, Properties of Vacuum Sintered Duplex Stainless Steels, *J. Mater. Process. Technol.*, 2005, **162-163**, p 286-292
7. G.S. Pradyot Datta, Upadhyaya, Sintered Duplex Stainless Steels from Premixes of 316L and 434L Powders, *Mater. Chem. Phys.*, 2001, **67**, p 234-242
8. M. Morakotjinda, N. Kuljittipipat, N. Poolthong, N. Tosangthum, P. Wila, R. Krataitong, T. Yodkaew, O. Coovattanachai, B. Vetayanugul, and R. Tongsri, Sintered Materials Prepared from Stainless Steel Series 300 and 400 Powders, *J. Met. Mater. Miner.*, 2008, **18**(1), p 69-74
9. M. Rosso, M. Actis Grande, and D. Ornato, Sintering of Duplex Stainless Steels and Their Properties, *Powder Metall. Prog.*, 2002, **2**, p 10-17
10. F. Martin, C. García, Y. Blanco, and M.L. Aparicio, Tribocorrosion Behavior of Powder Metallurgy Duplex Stainless Steels Sintered in Nitrogen, *Tribol. Int.*, 2013, **57**, p 76-85

11. L.A. Dobrzañski, Z. Brytan, M. Actis Grande, and M. Rosso, Properties of Duplex Stainless Steels Made by Powder Metallurgy, *Arch. Mater. Sci. Eng.*, 2007, **28**, p 217-223
12. M. Campos, A. Bautista, D. Cáceres, J. Abenojar, and J.M. Torralba, Study of the Interfaces Between Austenite and Ferrite Grains in P/M Duplex Stainless Steels, *J. Eur. Ceram. Soc.*, 2003, **23**, p 2813-2819
13. S.K. Mukherjee and G.S. Upadhyaya, Mechanical Behaviour of Sintered Ferritic Stainless steel-Al_2O_3 Particulate Composites Containing Ternary Additions, *Mater. Sci. Eng.*, 1985, **75**, p 67-78
14. S.C. Tjong and K.C. Lau, Abrasion Resistance of Stainless-Steel Composites Reinforced with Hard TiB_2 Particles, *Compos. Sci. Technol.*, 2000, **60**, p 1141-1146
15. S.C. Tjong and K.C. Lau, Sliding Wear of Stainless Steel Matrix Composite Reinforced with TiB Particles, *Mater. Lett.*, 1999, **4**, p 153-158
16. S.J. Lin and W.H. Xiong, Microstructure and Abrasive Behaviors of TiC-316L Composites Prepared by Warm Compaction and Microwave Sintering, *Adv. Powder Technol.*, 2012, **23**, p 419-425
17. F. Akhtar and S.J. Guo, Microstructure, Mechanical and Fretting Wear Properties of TiC-stainless Steel Composites, *Mater. Charact.*, 2008, **59**, p 84-90
18. E. Pagounis and V.K. Lindroos, Processing and Properties of Particulate Reinforced Steel Matrix Composites, *Mater. Sci. Eng. A*, 1998, **246**, p 221-234
19. Jayant Jain, Ashish M. Kar, and Anish Upadhyaya, Effect of YAG Addition on Sintering of P/M 316L and 434L Stainless Steels, *Mater. Lett.*, 2004, **58**, p 2037-2040
20. Q.L. Wu, W.G. Li, and N. Zhong, Corrosion Behavior of TiC Particle-Reinforced 304 Stainless Steel, *Corros. Sci.*, 2011, **53**, p 4258-4264
21. J. Kaziora, M. Nykiela, T. Pieczonkab, T. Marcu Puscasc, and A. Molinaric, Activated Sintering of P/M Duplex Stainless Steel Powders, *J. Mater. Process. Technol.*, 2004, **157-158**, p 712-717
22. M.A. El Saeed, F.A. Deorsola, and R.M. Rashad, Influence of SPS Parameters on the Density and Mechanical Properties of Sintered Ti_3SiC_2 Powders, *Int. J. Refract. Met. Hard Mater.*, 2013, **41**, p 48-53
23. D.P. Xiang, L. Ding, Y.Y. Li, J.B. Li, X.Q. Li, and C. Li, Microstructure and Mechanical Properties of Fine-Grained W-7Ni-3Fe Heavy Alloy by Spark Plasma Sintering, *Mater. Sci. Eng. A*, 2012, **551**, p 95-99
24. T. Borkar and R. Banerjee, Influence of Spark Plasma Sintering (SPS) Processing Parameters on Microstructure and Mechanical Properties of Nickel, *Mater. Sci. Eng. A*, 2014, **618**, p 176-181
25. S. Wei, Z.H. Zhang, F.C. Wang, X.B. Shen, H.N. Cai, S.K. Lee, and L. Wang, Effect of Ti Content and Sintering Temperature on the Microstructures and Mechanical Properties of TiB Reinforced Titanium Composites Synthesized by SPS Process, *Mater. Sci. Eng. A*, 2013, **560**, p 249-255
26. R. Mariappan, S. Kumaran, and T. Srinivasa Rao, Effect of Sintering Atmosphere on Structure and Properties of Austeno-Ferritic Stainless Steels, *Mater. Sci. Eng. A*, 2009, **517**, p 328-333
27. C. García, F. Martín, Y. Blanco, M.P. de Tiedra, and M.L. Aparicio, Corrosion Behaviour of Duplex Stainless Steels Sintered in Nitrogen, *Corros. Sci.*, 2009, **51**, p 76-86
28. C.J. Múnez, M.V. Utrilla, and A. Ureña, Effect of Temperature on Sintered Austeno-Ferritic Stainless Steel Microstructure, *J. Alloys Compd.*, 2008, **463**, p 552-558
29. I. Toor, J. Ahmed, M.A. Hussein, and N. Al-Aqeeli, Optimization of Process Parameters for Spark Plasma Sintering of Nano-structured Ferritic Fe-18Cr-2Si Alloy, *Powder Technol.*, 2016, **299**, p 62-70
30. L.A. Dobrzańnski, Z. Brytan, M. Actis Grande, and M. Rosso, Corrosion Behavior of Vacuum Sintered Duplex Stainless Steels, *J. Mater. Process. Technol.*, 2007, **191**, p 161-164